

Transgenic and mutant fly stocks	Key reference or source
<i>HB9-Gal4</i>	Thor et al., 1999
<i>ftz-Gal4</i>	Thor et al., 1999
<i>BG57-Gal4</i>	Budnik, 1996
<i>OK6-Gal4</i>	Landgraf et al., 2003
<i>D42-Gal4</i>	Landgraf et al., 2003
<i>UAS-mCD8-GFP</i>	Lee and Luo, 1999
<i>UAS-lamp-EGFP</i>	Pulipparacharuviil et al., 2005
<i>UAS-spin-GFP</i>	Sweeney and Davis, 2002
<i>UAS-shrb-GFP</i>	Sweeney et al., 2006
<i>UAS-MAD-GFP</i>	Dudu et al., 2006
<i>UAS-Rab7^{O67L}</i>	Entchev et al., 2000
<i>UAS-Rab5^{O88L}</i>	Entchev et al., 2000
<i>UAS-Rab5^{S43N}</i>	Entchev et al., 2000
<i>wah^{P1} = P{lacW}I(3)S009413</i>	Deák et al., 1997
<i>wah^{P2} = P{PZ}I(3)06536</i>	Spradling et al., 1999
<i>UAS-wah^{IR} (4699 R2-III; sterile homozygous females)</i>	National Institute of Genetics Stock Center (Mishima Japan)
<i>UAS-eIF4AIII-GFP</i>	unpublished
Antibodies and their concentration	Key reference or source
anti-Synapsin (3C11; mouse); 1:10	Developmental Studies Hybridoma Bank
anti-conjugated mono- and poly-ubiquitin (FK2; mouse); 1:50	Biomol
anti-Medea (rabbit); 1:1000	Sutherland et al., 2003
anti-phospho-MAD	Tanimoto et al., 2000
anti-Rab5 (rabbit); 1:500	Wucherpfennig et al., 2003
anti-Hrs (guinea pig); 1:500	Lloyd et al., 2002
anti-HA (3F10; rat); 1:50	Roche
anti-HRP/FITC (guinea pig); 1:200	Jackson labs
FITC-, TRITC- and Cy5-labelled secondary antibodies (donkey); 1:200	Jackson Laboratories

Tab. S1 Fly stocks and antibodies used in this study.

Fig. S1. Molecular characterisation of *wah*. **(A)** Genomic structure of *CG4699/wah* showing introns as dashed lines (not to scale) and numbered exons (<http://flybase.org/>). Non-coding exon regions are in black and coding exons in alternating light and dark grey. The three predicted splice versions (*wah*-RA,-RB,-RC) differ only in the length of exon 1 and encode therefore the same predicted protein of 1570 amino acid residues. Two lethal P-element insertions in the 5' untranslated region of *CG4699*, *P{lacW}I(3)S009413 (wah^{P1}*; sequence accession FM986317) and *P{PZ}I(3)06536 (wah^{P2}*; sequence accession AQ034070), fail to complement each others lethality (not shown). **(B)** Schematic representations of *wah*-RB transcript (1), Wah protein (2, 5), human KIAA1267 protein (3) and human AAI26156 protein (4). For the Wah protein (2, 5) positions of the PEHE domain (Marin, 2003), the histone fold domain (according to Ensembl; www.ensembl.org) and predicted nuclear localisation signals (*; according to PSORT; <http://psort.nibb.ac.jp/form2.html>) are indicated; connecting dashed lines show regions of sequence homology (alternative predictions for domain delineations indicated by slash) for the following pairings: Wah versus human KIAA1267 protein (dotted and dashed boxes), human KIAA1267 versus human AAI26156 (white boxes), human AAI26156 versus Wah (black bars); percentages of homology (identity/positives) are listed in boxes between protein pairs. The *wah^{IR}* fragment and probes for in situ hybridisations are indicated. **(C-F)** In situ hybridisation (based on alkaline phosphatase staining following standard protocols) (Plickert et al., 1997; Tautz and Pfeifle, 1989) to wild type (wt) and *wah^{P1}* mutant embryos at stages 12 and 16 (e12, e16) using the 3' probe as indicated in B; the central nervous system (asterisks) is strongly labelled in wild type at both stages, whereas staining outside the nervous system is visible at stage 12 but no longer at stage 16 (white arrows indicate the ventral musculature) – in agreement with the fact that no ubiquitin phenotypes are observed in late embryonic muscles (not shown); all staining is abolished in *wah^{P1}* embryos stained in the same batch as wild-type specimens, indicating staining to be specific. Scale bar (in A) represents 30 mm in all images.

Fig. S2. Effects of Wah loss-of-function on NMJ morphology. **A-C)** Images of NMJs (arrowheads) on ventral longitudinal muscles 3 and 4 (VL3/4; muscle nomenclature according to Bate, 1993) in late stage 17 embryos (e17) with different genotypes: wildtype, *wah^{P1}* mutant, or with targeted expression of *wah^{IR}* (driven in embryonic motoneurons by *Hb9-Gal4*). **(D)** Quantification of the relative lengths of embryonic NMJs on VL3/4 (NMJ lengths divided by respective muscle lengths; mean \pm SEM; n, number of terminals analysed; asterisks, $p \leq 0.002$ assessed by t-test); the *wah^{P1}* mutant phenotype is reproduced by motoneuronal expression of *wah^{IR}* in wildtype embryos and rescued by motoneuronal expression of *HA-wah* in *wah^{P1}* mutant embryos. **E-P)** Images of late larval (L3) NMJs (arrowheads) on different muscles (VL3/4, SBM, VO6); motoneurons at these NMJs are either wildtype (left), are *wah^{P1}* mutant (induced by MARCM mosaic strategy; middle), or display targeted expression of *wah^{IR}* (synchronously driven by the two larval motoneuronal drivers *OK6-Gal4* and *D42-Gal4*; right); the *wah^{P1}* mutation and knock-down of Wah cause comparable phenotypes: longer NMJs with normal bouton size on VL3/4 (E-G), smaller boutons but normal NMJ size on SBM (H-J), and no detectable phenotypes on muscle VO6 (K-P; one example of a small and one of a large NMJ are given, respectively). MARCM analysis was carried out as described previously (Lee and Luo, 1999; Vogler and Urban, 2008): two hour egg lays obtained from *hs-FLP¹²²; FRT82B, wah^{P1}/TM6b* females crossed to *elav-Gal4, hs-FLP¹/Y; UAS-mCD8-GFP; FRT82B, tub-Gal80* males were kept for 165 minutes at 25°C, heat shocked for 90 min at 37°C, and raised at 25°C into late third instar larvae. Female larvae (*hs-FLP¹²²/elav-Gal4, hsFLP¹; UAS-mCD8-GFP/+; FRT82B, tub-Gal80/FRT82B, wah^{P1}*) showing green fluorescent patches in the CNS were selected for dissection and stained. Stainings: act, phalloidin-stained F-actin; CD8, mCD8-GFP; Syn, Synapsin. Scale bar (in A) represents 15 mm in A-C, E-G, K-P, 50 mm in H-J.

Fig. S3. Selective co-accumulation of Hrs with differently induced ubiquitin puncta. Confocal images show horizontal views of late larval muscles expressing different constructs (indicated bottom left), stained against ubiquitin (Ubi, green) and Hrs (magenta). Hrs accumulated upon *wah^{IR}* but not *tau::myc* or *dts5* expression. Scale bar (in A) represents 50mm in all images; insets are 200% enlarged.

Fig. S4. Wah loss-of-function affects SMAD complex localisation in muscle nuclei. Late larval muscles of different genotypes (wt, wildtype; *GFP, UAS-eIF4AIII-GFP; wah^{IR}, UAS-wah^{IR}; mad-GFP, UAS-mad-GFP*; all constructs expressed with the muscle-specific driver *BG57-Gal4*), stained with antibodies against Medea (Med), phosphorylated Mothers against Dpp (pMad), ubiquitin (ubi) or visualised for GFP fluorescence. **(A-D)** Medea and p-MAD reliably accumulate in nuclei of wild-type muscles when dissected in PBS containing 500 nM Ca²⁺ (A,C); upon knock-down of Wah, nuclear levels of Medea or pMAD are suppressed (B,D); instead extranuclear patches of Medea can occasionally be seen that do not colocalise with ubiquitin puncta (close-up in B). **(E,F)** Nuclear Medea levels are rescued if *wah^{IR}* is co-expressed with *HA-wah*, but not with a *GFP* control construct. **(G,H)** Upon knock-down of Wah, Mad::GFP forms extracellular patches which do not overlap with ubiquitin puncta, confirming findings with anti-Medea; Mad::GFP enters nuclei even if Wah is knocked down, suggesting that the effect of *wah^{IR}* on SMAD complex localisation is not absolute. White arrowheads point at stained, open arrowheads at non-stained muscle nuclei. A,B,G,H represent confocal images, C-F were obtained on a conventional fluorescent microscope. Scale bar (in A) represents 50mm in A-F and 18 mm in G, H; insets are 200% enlarged.

Fig. S5. Sequences of cDNAs associated with different ESTs of *wah*. Schematic representation of *wah-RB* transcript, and sequences of cDNAs associated with different *wah* ESTs obtained for the cloning of the full-length *wah* gene. cDNAs were obtained from DGRC and sequenced multiple times. All sequences and annotations have been deposited with the following accession numbers: FM867599 (*SD06860*), FM867600 (*AT07776*), FM867601 (*AT22722*), FM867602 (*LD46639*) and FM867603 (*LD39557*). Different inconsistencies were found in most cDNAs, particularly in or around intron 5, and none represents a full-length cDNA. *SD06860* contains 50 bp from the first intron, part of the 5' UTR and all introns until it terminates at the *XhoI* site. *LP09056* starts at 1639 bp and covers the rest of the coding sequence and 3' UTR; it has a complete intron 5-6 sequence and a premature stop codon at 3859 bp. *AT07776/AT22722* contains 50 bp of the 5' UTR and covers 5 exons before terminating 60 bp into intron 5-6, followed by a poly A tail. *LD46639* contains the complete 5' UTR of isoform RA and terminates at the *XhoI* site; sequence contains 10 bp from intron 5-6. *LD39557* represents isoform RB including the complete 5' UTR, and terminates at the *XhoI* site; it lacks about 63 bp of exon 5.

Movie 1. Tomogram of sausage body fragment. Tomogram calculated from a tilt series of a 120 nm thick section through a sausage body; see Fig. 2 for still images and detailed explanations.

Movie 2. 3D reconstruction of a sausage body fragment. 3D reconstruction of the tomogram shown in movie 1; tubules forming continuous entities within the analysed fragment are colour coded distinctly; see Fig. 2 for still images and detailed explanations.

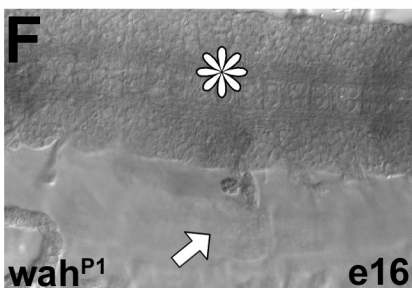
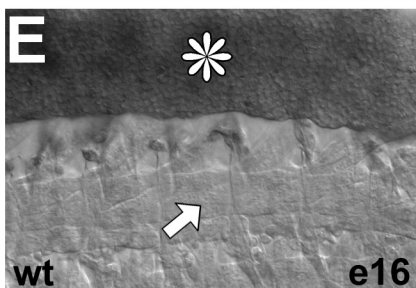
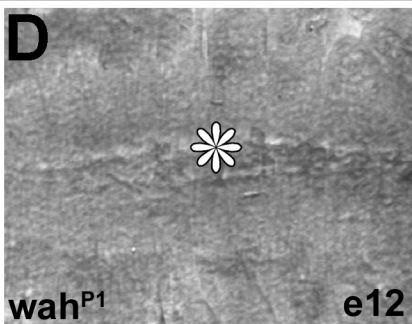
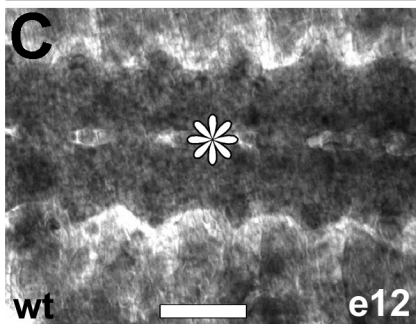
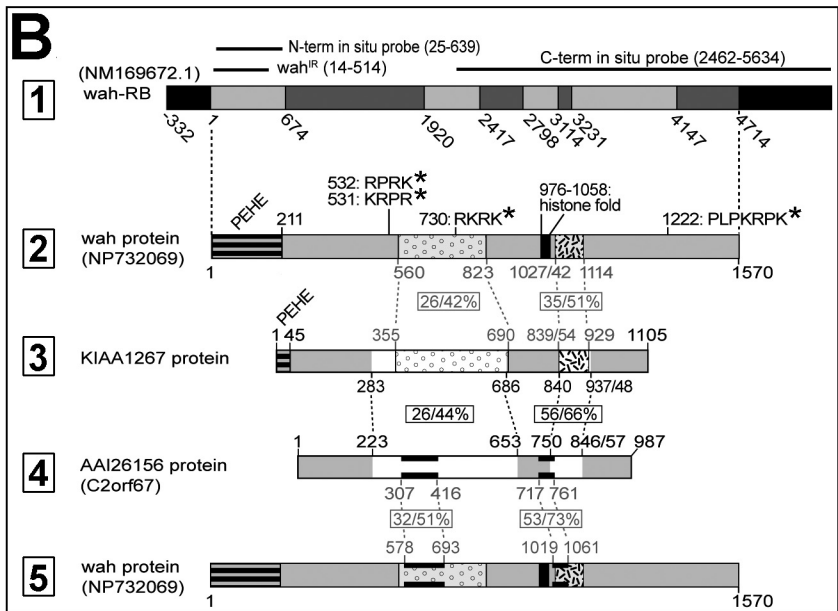
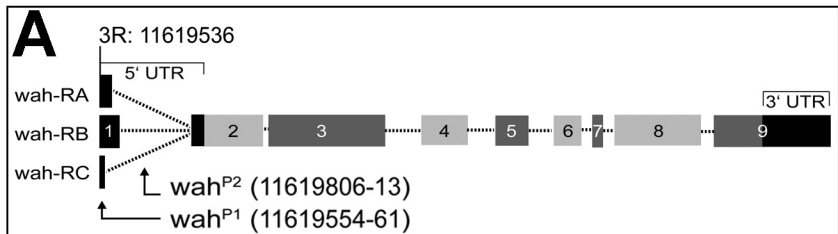


Fig.S1 Lone et al.

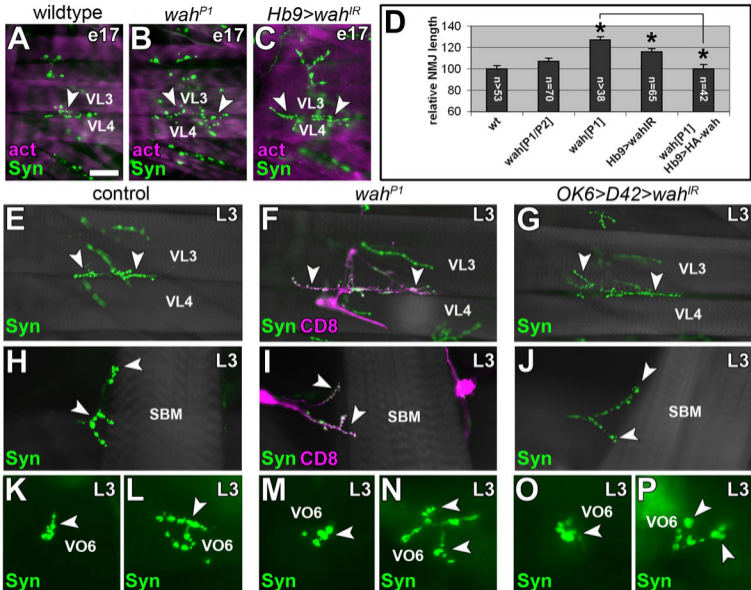


Fig. S2 Lone et al.

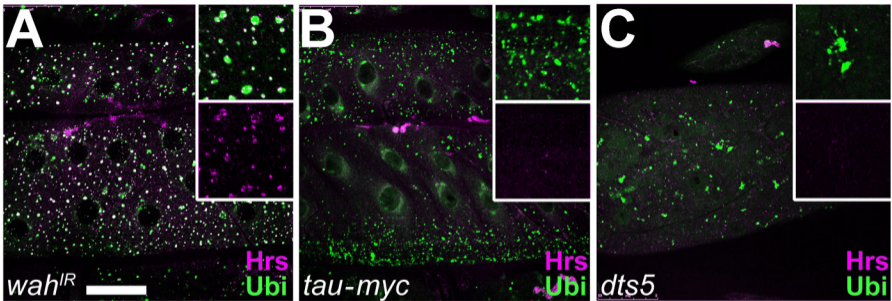


Fig. S3 Lone et al.

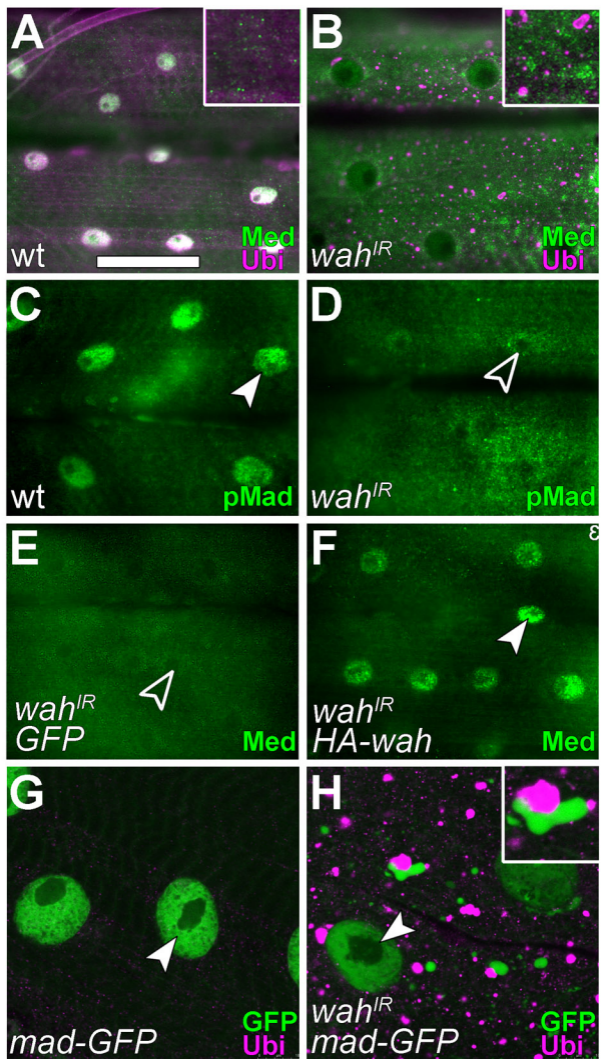
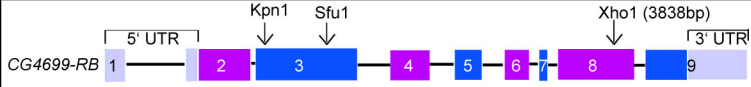


Fig. S4 Lone et al.



EST

cDNA

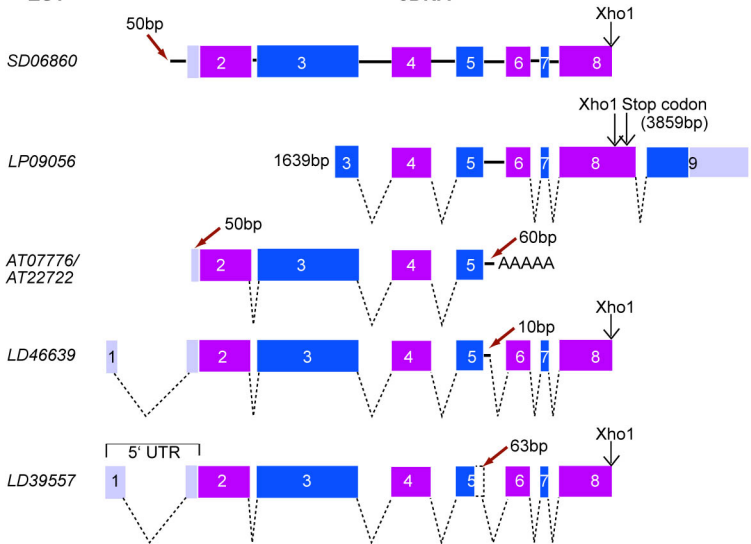


Fig. S5 Lone et al.